A Control Method Using Two Electromotive Forces and a Disturbance Observer to Improve the Dynamics of a Virtual Synchronous Machine

Geon Heo, *Graduate Student Member, IEEE*, Yongsoon Park, *Member, IEEE*, Kyungkyu Lee, and Hoseon Ryu

***Abstract*—The modern power grid is facing a significant challenge due to decreasing grid inertia, which is caused by the high penetration of renewable energy sources (RESs). Virtual synchronous machines (VSMs) have been considered as effective solutions to support the grid by providing inertial responses similar to that of traditional synchronous machines. However, fast and flexible dynamic responses to reference inputs, which can be achieved by conventional RES interfacing inverters, are degraded when inverters emulate the behavior of a synchronous machine. In this article, a current-referencing electrified synchronous machine (CURESYM) is proposed as a control method to adjust the dynamics to the reference input regardless of the parameter settings for emulating a synchronous generator. That is, the output current of CURESYM can be regulated with an intended dynamic response to follow the current reference. In addition, the accuracy of the current regulation can be enhanced by virtue of a disturbance observer. The fundamental characteristics of CURESYM are described with laboratory-scale experimental results. Finally, the effectiveness of CURESYM is discussed with practical data from on-site tests that applied the proposed method to a battery energy storage system in an actual island microgrid.**

***Index Terms*—Virtual synchronous machine, voltage-source inverter, battery energy storage system.**

I. Introduction

THE increasing need for a sustainable energy supply to defend against the climate crisis has brought about significant changes in the modern power grid. Traditionally, the stability of the power grid was primarily maintained by large synchronous generators of fossil-fuel plants. The inertial response provided by these synchronous machines contributes significantly to maintaining the grid frequency at its nominal value. However, the gradual retirement of synchronous generators in the process of replacing fossil-fuel plants with renewable energy sources (RESs) has led to a reduction of the grid inertia, thereby deteriorating the frequency stability of the grid [1], [2], [3].

Many RESs are connected to the grid through voltage-source inverters. These inverters are generally sorted into two categories: grid-following (GFL) and grid-forming (GFM) inverters [4]. GFL inverters are normally synchronized with the grid using a phase-locked loop (PLL), which estimates the frequency and phase angle of the grid voltage, and their output power is rapidly and strictly regulated according to the reference input with an inner current controller [5], [6]. Therefore, GFL inverters are considered as current sources in the grid and do not provide inertial response [7]. Conventional droop control can be combined with GFL inverters to support the grid frequency by changing their output power according to frequency deviations [8] [9]. However, the response time to a frequency deviation may be limited by the estimation delay of the PLL. In contrast, GFM inverters can more immediately respond to grid frequency variations than GFL inverters because they generate their own frequency and phase angle without a PLL [10]. As GFM inverters determine the magnitude and phase angle of their own output voltages, they can be regarded as voltage sources, akin to conventional synchronous machines. However, certain GFM inverters that use only droop control without an electromechanical model of a synchronous machine may not offer an inertial response explicitly [10], [11], [12].

Virtual synchronous machines (VSMs) are a type of GFM inverter based on a mathematical model of a synchronous machine [13], [14], [15], [16], [17], [18], [19], [20], [21], [22]. VSMs normally consist of a swing equation, droop control, and a simplified excitation system [13], [14]. The power responses of VSMs are primarily determined by the inertia and droop coefficients [15]. Specifically, the degree of the inertial response is changed by the inertia coefficient, and the load sharing of the VSM with respect to the frequency deviation is determined by the droop coefficient. However, at the same time, these coefficients are also associated with the transient response to the reference input change (RIC) of the VSM [21]. Therefore, if these parameters are

Manuscript received 14 March 2023; revised 25 June 2023 and 6 September 2023; accepted 8 October 2023. Date of publication 13 October 2023; date of current version 22 March 2024. This work was supported in part by the Korea Institute of Energy Technology Evaluation and Planning (KETEP) and the Ministry of Trade, Industry & Energy (MOTIE) of the Republic of Korea under Grant 20204010600340, and in part by Korea Electric Power Corporation under Grant CX72200088. Paper no. TSTE-00274-2023. *(Corresponding author: Yongsoon Park.)*

Geon Heo and Yongsoon Park are with the Gwangju Institute of Science and Technology, Gwangju 61005, South Korea (e-mail: dunamisheo@gm.gist.ac.kr; yongsoon@gist.ac.kr).

Kyungkyu Lee and Hoseon Ryu are with Korea Electric Power Research Institute, Daejeon 520-350, South Korea (e-mail: kk.lee@kepco.co.kr; hoseon.ryu@kepco.co.kr).

Color versions of one or more figures in this article are available at https://doi.org/10.1109/TSTE.2023.3324382.

Digital Object Identifier 10.1109/TSTE.2023.3324382

TABLE I
COMPARISONS OF VSGS IN TERMS OF DYNAMICS

Method	Droop & Damping	Regulation dynamics & inertial and damping response	Parameters related to the regulation dynamics
Synchronverter [13], [14]	Combined	Combined	Inertia and droop coefficients
Adaptive parameters [15]-[17]	Combined	Combined	Inertia and droop coefficients
Transient damping [19]-[22]	Separated	Combined	Inertia, droop, and damping coefficients, and other filtering parameters
CURESYM	Separated	Separated	Current modulating time constant

mainly designed for the inertial response and load sharing, the dynamic response to the RIC may be compromised. For instance, active power variations to the RIC may have large oscillations and long settling times depending on the inertia coefficient [16].

To acquire a desirable response to the RIC, the inertia and the droop coefficients can be adaptively adjusted when the system is in a transient state [15], [16], [17]. This sort of adaptive method commonly adjusts those parameters to improve the dynamics of the VSM when connected to an infinite bus. However, these parameters should be carefully determined by considering the grid stability as well. Otherwise, nonlinear parameter changes may exacerbate other electromechanical modes and deteriorate the stability of the power system [18].

Another method by which to improve the RIC dynamics is to use an additional damping component, the effects of which only appear during transient states regardless of the droop coefficient [19], [20], [21], [22]. In earlier work [19], an external frequency measurement is used to separate the damping response from the droop response, and the damping coefficient can be designed to mitigate transient power oscillations. The transient damping effect can also be achieved by using a high-pass-filtered rotor frequency without an external frequency measurement [20]. This method effectively emulates the damping effect from the damper winding in a conventional synchronous machine. Alternatively, an additional damping component can be obtained from the ratio of the torque to the flux linkage [21] or by imitating a power system stabilizer (PSS) [22]. To a degree, the additional damping components are deemed effective in mitigating power oscillations because they offset the detrimental impact of the droop coefficient on the RIC dynamics. However, as the damping components are related to the frequency deviation, it is difficult to offset the impact of the inertia coefficient, which is associated with the frequency derivative. Therefore, a novel method insensitive to not only the droop coefficient but also the inertia coefficient should be derived for the RIC dynamics.

In this article, a current-referencing electrified synchronous machine (CURESYM) is proposed as a solution to these problems. Fundamentally, CURESYM generates two electromotive forces (EMFs) with different roles from one another. One is responsible for regulating the output current with a desired dynamic response, and the other emulates the electromechanical behaviors of a synchronous machine. In CURESYM, the dynamic response to the current reference can be separately designed without being affected by the other parameters to emulate the behaviors of synchronous machines. Consequently, CURESYM can achieve rapid and flexible regulation approximating those of conventional GFL inverters. The accuracy of the current regulation can be ensured in combination with a disturbance observer. This combination allows the proposed method to operate as a current source under an ideally undistorted grid. However, when the grid frequency is disrupted, CURESYM can offer an inertial response simultaneously. Furthermore, when using the proposed method, the transient damping response is adjustable regardless of the droop control. Some comparisons of the existing VSGs, including CURESYM, are summarized in Table I. It can be seen that CURESYM has the advantage of being able to separately adjust responses to various functions of VSG. In other words, the performances of inertial and damping responses, load sharing, and RIC dynamics in the proposed method can be designed through independent control variables for each function.

The remainder of this article is organized as follows. Section II describes the overall structure and basic concepts of the proposed CURESYM. Section III explains detailed implementation methods of CURESYM. Section IV demonstrates the characteristics of CURESYM with experimental results. In Section V, the effectiveness of proposed control method is discussed with on-site test results. CURESYM's algorithm was tested in the 250kW inverter of a battery energy storage system (BESS) installed in an island grid with low inertia. Finally, Section VI concludes this article.

II. OVERALL SYSTEM DESCRIPTION

Fig. 1 presents an overall system description of CURESYM. A three-phase voltage-source inverter with an output LC filter is considered in this article. A BESS is connected to the DC-link of the inverter as a voltage source. Similar to earlier work [13], the inverter can be considered equivalent to a synchronous machine with small static condensers connected in parallel to the terminals of the armature windings. Comparing the inverter to a synchronous machine, the filter inductor, whose inductance and resistance are respectively L_f and R_f, corresponds to the armature winding. Hence, the inverter's output current $\mathbf{i}_{abc}(=[i_a \quad i_b \quad i_c]^T)$ is considered as the armature current. The output voltage of the inverter $\mathbf{e}_{abc}(=[e_a \quad e_b \quad e_c]^T)$ synthesized by pulse-width modulation (PWM) corresponds to the EMF of the synchronous machine, and the grid voltage $\mathbf{v}_{abc}(=[v_a \quad v_b \quad v_c]^T)$ corresponds to the terminal voltage of the armature windings.

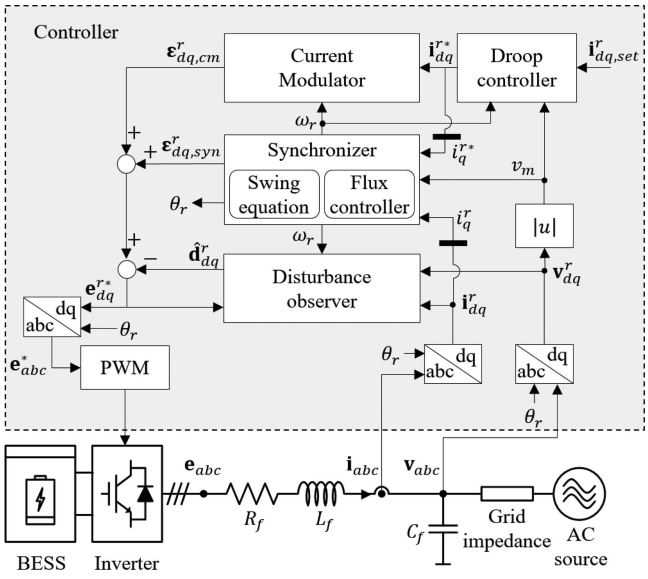

Fig. 1. Overall system description. Inverter.

The control algorithms for CURESYM consist of a current modulator, a synchronizer, and a disturbance observer. First, the current modulator generates current-modulating EMF (CMEMF), denoted by $\boldsymbol{\varepsilon}^r_{dq,cm}(=\begin{bmatrix}\varepsilon^r_{d,cm} & \varepsilon^r_{q,cm}\end{bmatrix}^T)$ in the synchronous reference frame (SRF), which allows the inverter's output current to follow the current reference with a desired dynamic response. Fundamentally, the control algorithms for CURESYM are implemented in the SRF. The current generated by CMEMF mainly determines the output current level in the steady-state region. Second, the synchronizer generates synchronizing EMF (SEMF), denoted by $\boldsymbol{\varepsilon}^r_{dq,syn}(=\begin{bmatrix}\varepsilon^r_{d,syn} & \varepsilon^r_{q,syn}\end{bmatrix}^T)$, which emulates the characteristics of the conventional synchronous machine. The angular frequency ω_r and the phase angle θ_r used for coordinate transformation are generated from the synchronizer. The synchronizer is based on a swing equation representing the mechanical behavior of the synchronous machine and a flux controller operating as a virtual excitation system. The current generated by SEMF is superimposed on the current generated by CMEMF. Finally, the disturbance observer improves the control accuracy by compensating for disturbances caused by parameter errors and the nonlinearity of the inverter.

Fundamentally, the desired response to the output current of CURESYM is described in the frequency domain as follows:

$$\mathbf{i}^r_{dq} = \begin{bmatrix}\frac{1}{\tau_{cm}s+1} & 0\\ 0 & \frac{1}{\tau_{cm}s+1}\end{bmatrix}\mathbf{i}^{r*}_{dq} + \begin{bmatrix}R_f+sL_f & -\omega_r L_f\\ \omega_r L_f & R_f+sL_f\end{bmatrix}^{-1}\left(\boldsymbol{\varepsilon}^r_{dq,syn}-\mathbf{v}^r_{dq}\right), \quad (1)$$

where 's' is the Laplace operator and $\mathbf{i}^{r*}_{dq}(=\begin{bmatrix}i^{r*}_d & i^{r*}_q\end{bmatrix}^T)$ is the current reference in the SRF. Hereafter, the superscript '$*$' denotes the reference value. In addition, $\mathbf{i}^r_{dq}(=\begin{bmatrix}i^r_d & i^r_q\end{bmatrix}^T)$ and

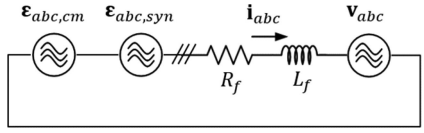

Fig. 2. Equivalent circuit of CURESYM.

$\mathbf{v}^r_{dq}(=\begin{bmatrix}v^r_d & v^r_q\end{bmatrix}^T)$ are obtained correspondingly from $\mathbf{i}_{abc}$ and $\mathbf{v}_{abc}$ by Park's transformation method.

According to (1), two factors determine the output current of CURESYM. The first is $\mathbf{i}^{r*}_{dq}$ and the second is the voltage vector difference between $\boldsymbol{\varepsilon}^r_{dq,syn}$ and $\mathbf{v}^r_{dq}$. The response to $\mathbf{i}^{r*}_{dq}$ has first-order dynamics for which the time constant is τ_{cm}, as described in the first term on the right-hand side of (1). This dynamic response is scarcely affected by other factors, such as the inertia coefficient. The second term on the right-hand side of (1) represents the current flowing through the filter inductor caused by the voltage vector difference between $\boldsymbol{\varepsilon}^r_{dq,syn}$ and $\mathbf{v}^r_{dq}$. This vector difference is caused by the phase angle difference governed by the dynamics of the swing equation and the magnitude difference due to the response of the flux controller. The voltage vector difference is normally held at zero in a steady state by a synchronizer.

Simply, CURESYM can be represented by the three-phase equivalent circuit described in Fig. 2 when using an average model of the inverter and assuming ideal conditions without any disturbances. Here, $\boldsymbol{\varepsilon}_{abc,cm}$ and $\boldsymbol{\varepsilon}_{abc,syn}$ are the inverse Park's transformations of $\boldsymbol{\varepsilon}^r_{dq,cm}$ and $\boldsymbol{\varepsilon}^r_{dq,syn}$, respectively. The inverter side is regarded as two voltage sources connected in series. In the nominal condition, where the grid frequency and voltage are constant, $\boldsymbol{\varepsilon}_{abc,syn}$ and $\mathbf{v}_{abc}$ cancel each other out because their vector difference is zero. Hence, $\mathbf{i}_{abc}$ is only controlled by $\boldsymbol{\varepsilon}_{abc,cm}$ originated from the current reference. However, if $\mathbf{v}_{abc}$ fluctuates due to a generator trip or a sudden load change, the difference between $\boldsymbol{\varepsilon}_{abc,syn}$ and $\mathbf{v}_{abc}$ may not be negligible. As a result, the output current can respond to such a difference as grid support even if the current reference is fixed. In the following sections, the implementation of each component of CURESYM is detailed and how CURESYM achieves the response shown in (1) is explained.

III. Implementation of CURESYM

A. Current Modulator

The current modulator generates CMEMF to control the output current of CURESYM according to $\mathbf{i}^{r*}_{dq}$. If SEMF and the grid voltage in Fig. 2 are deactivated by the superposition principle to consider only the effect of CMEMF, CMEMF of the dq-axes in the SRF can be calculated based on the voltage equations below:

$$\begin{cases}\varepsilon^r_{d,cm} = R_{fn}\tilde{i}^r_d + L_{fn}\frac{d\tilde{i}^r_d}{dt} - \omega_r L_{fn}\tilde{i}^r_q\\ \varepsilon^r_{q,cm} = R_{fn}\tilde{i}^r_q + L_{fn}\frac{d\tilde{i}^r_q}{dt} + \omega_r L_{fn}\tilde{i}^r_d\end{cases}. \quad (2)$$

In these equations, $\tilde{i}^r_d$ and $\tilde{i}^r_q$ are the desired current traces of the dq-axes in the SRF, and R_{fn} and L_{fn} are nominal parameters

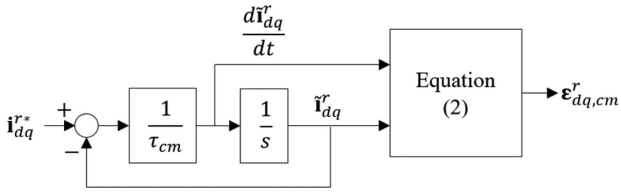

Fig. 3. Current modulator.

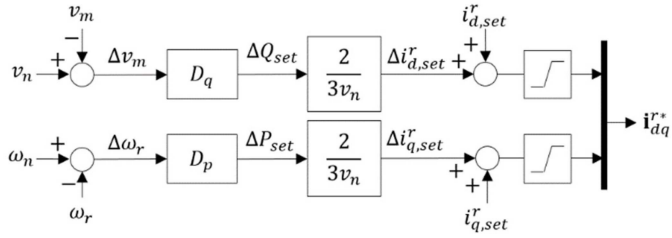

Fig. 4. Droop controller for CURESYM.

of the L-filter. When the current traces are simply designed as the response of a first-order system to $\mathbf{i}^{r*}_{dq}$, as in a conventional proportional-integral (PI) control-based current controller [23], the current modulator is implemented as described in Fig. 3. Given that the derivative of $\tilde{\mathbf{i}}^r_{dq}$ is obtained from the input of the integrator, the direct differential operations in (2) can be avoided, which are normally vulnerable to noise in digital implementations. When using Fig. 3, the actual output current $\mathbf{i}^r_{dq}$ may coincide with $\tilde{\mathbf{i}}^r_{dq}$ through CMEMF. However, the errors between nominal and actual parameters and nonlinearity of the inverter [24] may cause control errors in practical situations. This limitation can be improved by a disturbance observer, as explained later.

With CURESYM, the droop controller is implemented by changing $\mathbf{i}^{r*}_{dq}$ with respect to the angular frequency deviation and the magnitude deviation of the grid voltage. As shown in Fig. 4, ΔP_{set} and ΔQ_{set} are generated using conventional $\omega - P$ and $V - Q$ droop equations in advance [8]. Then, ΔP_{set} and ΔQ_{set} are transformed into the current change references $\Delta i^r_{d,set}$ and $\Delta i^r_{q,set}$ according to the instantaneous power theory [9]. When calculating current change references, the magnitude of the grid voltage is approximated to the nominal value v_n for smooth variations of the current references. In addition, it is assumed that the grid voltage only exists on the q-axis, as the phase angles of CURESYM and the grid voltage are usually synchronized. The errors from these approximations are normally negligible in practical implementations. After the current set-points $i^r_{d,set}$ and $i^r_{q,set}$ are added to the current change references, $\mathbf{i}^{r*}_{dq}$ is finally calculated.

B. Synchronizer

The synchronizer is implemented to mimic the behavior of a two-pole round rotor machine. The frequency of CURESYM is synchronized with the grid frequency through the synchronizer. If the SRF is defined such that the rotor flux is aligned with the direct axis, SEMF calculated from the synchronizer is derived

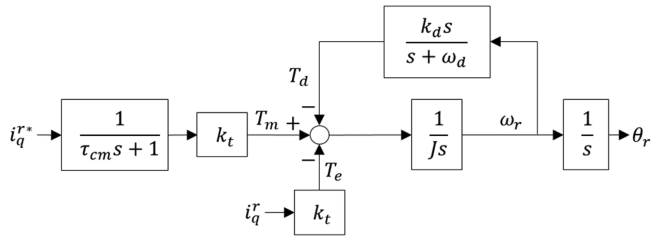

Fig. 5. Mechanical part of the synchronizer.

as follows:

$$\boldsymbol{\varepsilon}^r_{dq,syn} = [0 \quad \omega_r \lambda_f]^T. \tag{3}$$

Here, λ_f is the imaginary flux linkage. The phase angle and magnitude of $\boldsymbol{\varepsilon}^r_{dq,syn}$ are synchronized to those of the grid voltage. The synchronization of the phase angle is achieved by the mechanical part of the synchronizer described in Fig. 5. The mechanical part is based on the swing equation:

$$J\frac{d\omega_r}{dt} = T_m - T_e - T_d, \tag{4}$$

where J is the inertia of the imaginary rotor and T_d is the damping torque. Furthermore, T_m and T_e are the mechanical and electromagnetic torque values, respectively. The damping torque is calculated with the high-pass filtered angular frequency and can be described in the Laplace domain:

$$T_d = \frac{s}{s+\omega_d} k_d \omega_r. \tag{5}$$

Here, k_d is the damping coefficient and ω_d is the cut-off frequency of the high-pass filter (HPF). The damping torque in (5) represents the damping effect of the damper winding in a synchronous machine [20]. Hence, T_d appears only in the transient state and acts in the direction of suppressing changes in the angular frequency. Because it is assumed that the SRF is aligned with the rotor flux, T_e can be expressed as

$$T_e = k_t i^r_q = 1.5\lambda_f i^r_q, \tag{6}$$

where k_t is the torque constant. Similarly, T_m is calculated through the q-axis current reference as follows:

$$T_m = k_t i^{r*}_q \frac{1}{\tau_{cm}s+1}. \tag{7}$$

Hence, T_m acts as the torque reference of CURESYM. It should be noted that T_m contains the first-order delay whose time constant is τ_{cm}. This delay is designed for the decoupling of the current modulator and synchronizer. When i^{r*}_q is given, i^r_q may change with the first-order response due to the current modulator. By including the same delay in (7), T_m and T_e cancel each other out as i^{r*}_q varies.

A phase difference between the synchronizer and the grid voltage during any grid event causes CURESYM to provide the inertial response to the grid. After a grid event occurs, ω_r swings until T_e converges to T_m and synchronizes with the grid frequency again in a steady state. In a conventional synchronous machine, there exists a load angle at which T_e is not zero in a

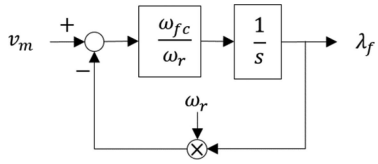

Fig. 6. Flux controller.

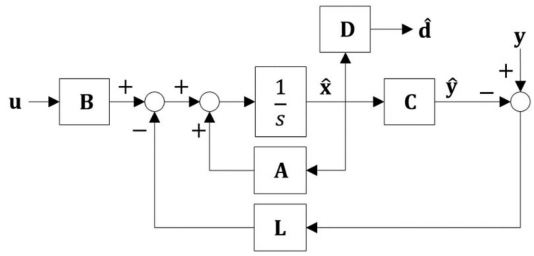

Fig. 7. Disturbance observer to compensate for uncertainties of CURESYM.

steady state. In other words, a phase difference between the EMF of the synchronous machine and the grid voltage contributes to generating electrical torque. However, the phase angle of the synchronizer in CURESYM always converges to that of the grid voltage in a steady state because the EMF of CURESYM is calculated as the sum of CMEMF and SMEMF. The load angle of CURESYM in a steady state is mainly determined by the phase of CMEMF.

Magnitude synchronization of $\boldsymbol{\varepsilon}^r_{dq,syn}$ is achieved by the flux controller described in Fig. 6. The flux controller adjusts λ_f such that $\omega_r\lambda_f$ follows v_m $(= |\mathbf{v}^r_{dq}|)$. The closed-loop transfer function of the flux controller can be derived as

$$G_{fc}(s) = \frac{\omega_r\lambda_f}{v_m} = \frac{\omega_{fc}}{s+\omega_{fc}}. \tag{8}$$

The dynamic response of the flux controller is determined by the flux control bandwidth ω_{fc}. Even if the phase angles of $\boldsymbol{\varepsilon}^r_{dq,syn}$ and $\mathbf{v}^r_{dq}$ are matched by the mechanical part after a grid event, the q-axis component of $\boldsymbol{\varepsilon}^r_{dq,syn} - \mathbf{v}^r_{dq}$ retains a non-zero value unless magnitude synchronization is completed. However, the non-zero q-axis voltage difference leads to both d-axis and q-axis currents as inferred from the second term on the right side of (1). Although the steady-state output powers are mainly controlled by $\mathbf{i}^{r*}_{dq}$ in CURESYM, the role of the synchronizer is important for accurate power control.

By calculating the voltage reference $\mathbf{e}^{r*}_{dq}$ as the sum of $\boldsymbol{\varepsilon}^r_{dq,cm}$ in (2) and $\boldsymbol{\varepsilon}^r_{dq,syn}$ in (3), the response of the output current described in (1) can be achieved. If CURESYM is connected to a stable grid, $\boldsymbol{\varepsilon}^r_{dq,syn} - \mathbf{v}^r_{dq}$ is usually nullified and the output current is only determined by $\mathbf{i}^{r*}_{dq}$. However, when the grid frequency fluctuates, the phase difference between $\boldsymbol{\varepsilon}^r_{dq,syn}$ and $\mathbf{v}^r_{dq}$ starts to generate a current flow. This current is related to the inertial response of CURESYM.

C. Disturbance Observer

In a practical system, uncertainties inevitably exist, and their effects can be modeled as a lumped disturbance applied to the system [25]. In CURESYM, such uncertainties may occur due to modeling errors of the inductive filter and the inverter nonlinearity. As mentioned earlier, because the current modulator has an open-loop control structure, the control accuracy may be degraded by disturbances from uncertainties. A block diagram of the disturbance observer is given in Fig. 7.

When the disturbances are regarded as voltage distortions on the inverter side, the circuit equation based on Fig. 1 is derived in the SRF as follows:

$$\begin{aligned} e^{r*}_d + d^r_d &= R_{fn}i^r_d - \omega_r L_{fn} i^r_q + L_{fn}\frac{di^r_d}{dt} + v^r_d \\ e^{r*}_q + d^r_q &= R_{fn}i^r_q + \omega_r L_{fn} i^r_d + L_{fn}\frac{di^r_q}{dt} + v^r_q. \end{aligned} \tag{9}$$

Here, d^r_d and d^r_q are the disturbances from the uncertainties. If one of the nominal parameters in (9) differs from the actual counterpart, the observer considers this difference as one of the disturbances to be offset. As described in Fig. 1, the voltage reference $\mathbf{e}^{r*}_{dq}(= \begin{bmatrix} e^{r*}_d & e^{r*}_q \end{bmatrix}^T)$ is the sum of the estimated disturbance $\hat{\mathbf{d}}^r_{dq}(= \begin{bmatrix} \hat{d}^r_d & \hat{d}^{r*}_q \end{bmatrix}^T)$, SEMF $\boldsymbol{\varepsilon}^r_{dq,syn}$, and CMEMF $\boldsymbol{\varepsilon}^r_{dq,cm}$. If the disturbances are precisely offset by $\hat{\mathbf{d}}^r_{dq}$, the desired response of CURESYM described in (1) can be achieved through CMEMF and SEMF. In this article, an extended state observer (ESO), a type of disturbance observer, is used to estimate and compensate for disturbances [25], [26]. To design the ESO, a state equation based on (9) is derived as shown below, including disturbances in the state vector $\mathbf{x}$.

$$\frac{d}{dt}\mathbf{x} = \mathbf{A}\mathbf{x} + \mathbf{B}\mathbf{u} \tag{10a}$$

$$\mathbf{y} = \mathbf{C}\mathbf{x}, \tag{10b}$$

where

$$\mathbf{A} = \begin{bmatrix} -R_{fn}/L_{fn} & \omega_r & 1/L_{fn} & 0 \\ -\omega_r & -R_{fn}/L_{fn} & 0 & 1/L_{fn} \\ 0 & 0 & 0 & 0 \\ 0 & 0 & 0 & 0 \end{bmatrix} \tag{10c}$$

$$\mathbf{B} = \begin{bmatrix} 1/L_{fn} & 0 & 0 & 0 \\ 0 & 1/L_{fn} & 0 & 0 \end{bmatrix}^T \tag{10d}$$

$$\mathbf{C} = \begin{bmatrix} 1 & 0 & 0 & 0 \\ 0 & 1 & 0 & 0 \end{bmatrix} \tag{10e}$$

$$\mathbf{x} = \begin{bmatrix} i^r_d & i^r_q & d^r_d & d^r_q \end{bmatrix}^T \tag{10f}$$

$$\mathbf{u} = \mathbf{e}^{r*}_{dq} - \mathbf{v}^r_{dq} = \begin{bmatrix} e^{r*}_d - v^r_d \\ e^{r*}_q - v^r_q \end{bmatrix} \tag{10g}$$

$$\mathbf{y} = \begin{bmatrix} i^r_d & i^r_q \end{bmatrix}^T. \tag{10h}$$

Because the system represented in (10) is observable, an ESO can be designed as shown below.

$$\frac{d}{dt}\hat{\mathbf{x}} = \mathbf{A}\hat{\mathbf{x}} + \mathbf{B}\mathbf{u} + \mathbf{L}\left(\mathbf{y} - \mathbf{C}\hat{\mathbf{x}}\right) \tag{11a}$$

$$\mathbf{L} = \begin{bmatrix} l_1 & l_3 & l_5 & l_7 \\ l_2 & l_4 & l_6 & l_8 \end{bmatrix}^T. \tag{11b}$$

The hat symbol "^" indicates an estimated value. The observer gains in matrix $\mathbf{L}$ are designed to make the estimation error of the state vector converge to zero. The error dynamics of the state vector is described as

$$\frac{d}{dt}\left(\mathbf{x} - \hat{\mathbf{x}}\right) = \left(\mathbf{A} - \mathbf{LC}\right)\left(\mathbf{x} - \hat{\mathbf{x}}\right). \tag{12}$$

If the observer gains are chosen such that all eigenvalues of $\mathbf{A} - \mathbf{LC}$ are located on the left-half plane, the estimated disturbance can be obtained from the estimated state vector as follows:

$$\hat{\mathbf{d}}_{dq}^r = \mathbf{D}\hat{\mathbf{x}} \tag{13a}$$

$$\mathbf{D} = \begin{bmatrix} 0 & 0 & 1 & 0 \\ 0 & 0 & 0 & 1 \end{bmatrix}. \tag{13b}$$

To make the observer structure symmetric in the SRF and place all poles simply at the same value ω_{eso}, the observer gains can be set as follows:

$$l_1 = 2\omega_{eso} - \frac{R_{fn}}{L_{fn}} \pm \omega_r \tag{14a}$$

$$l_4 = 2\omega_{eso} - \frac{R_{fn}}{L_{fn}} \mp \omega_r \tag{14b}$$

$$l_5 = l_8 = -\omega_{eso}^2 L_{fn} \tag{14c}$$

$$l_2 = l_3 = l_6 = l_7 = 0. \tag{14d}$$

Given that the estimation error of the observer is generally required to converge more rapidly than the other control dynamics, ω_{eso} should be sufficiently greater than the bandwidth of the flux controller and the current modulator.

The observer response can then be faster than the mechanical response of the synchronizer.

In summary, the combination of the disturbance observer and the current modulator can be regarded as a type of current feedback regulator. However, because the vector difference between the SEMF and the grid voltage is explicitly modeled as the input rather than as a disturbance in the disturbance observer, CURESYM can simultaneously represent the characteristics of the current regulator and the VSM.

IV. Experimental Results

A. Experimental Setup

Experiments were conducted to evaluate the performance of CURESYM with a three-phase voltage source inverter. Fig. 8 shows the overall experimental setup based on Fig. 1. The control

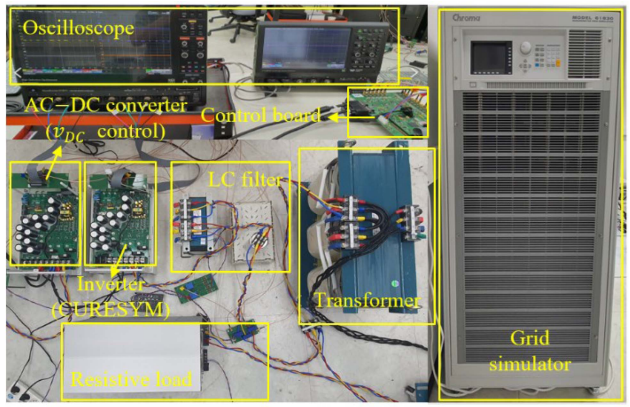

Fig. 8. Experimental setup.

TABLE II
Parameters Used for the Laboratory-Scale Experiments

	Parameter	Value
Circuit	Nominal grid frequency	60 Hz
	Nominal grid voltage (L-L)	220 V
	Nominal inverter power: S_n	11.4 kVA
	L_f	1.5 mH
	R_f	84 mΩ
	C_f (Δ-conn.)	16 μF
Default control parameters	J	0.2 kg · m^2
	k_d	3 N · m · s/rad
	ω_d	$2\pi \cdot 1$ rad/s
	τ_{cm}	100 ms
	ω_{fc}	$2\pi \cdot 100$ rad/s
	ω_{eso}	$2\pi \cdot 300$ rad/s
	D_p	$S_n/(0.03 \cdot 2\pi \cdot 60)$
	D_q	$\sqrt{3}S_n/(0.2 \cdot 220\sqrt{2})$

algorithm for CURESYM is implemented on a control board based on TMS320C28346 with a sampling frequency of 15 kHz. The DC-link voltage is regulated at 350 V. The inverter is connected to the grid simulator through an LC-filter and a transformer. The circuit parameters of the experimental setup are listed in Table II.

B. Response to Changes in the Current Reference

First, the response of CURESYM to a RIC was tested while the droop controller was not applied. The step response of CURESYM to the d-q current references is shown in Fig. 9. In this experiment, the d- and q-axis currents were initially held to zero and 10 A, respectively. In Fig. 9(a), 20 A step changes in the current references are sequentially applied for the q-axis and d-axis. Because the frequency and voltage magnitude of the grid simulator are fixed, the effect of SEMF was negligible.

Therefore, it can be observed that first-order responses with the intended time constants (τ_{cm}) occur for the current regulation on each axis. In addition, the d-and the q-axis current responses are decoupled from each other. Because the degree of voltage distortion caused by parameter errors or inverter nonlinearity can vary depending on the output current, the disturbance voltage

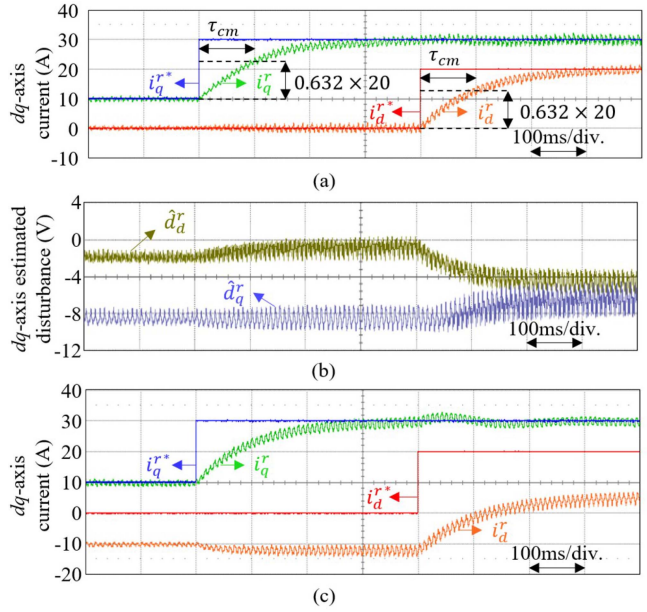

Fig. 9. Experimental result of the step response of CURESYM in the current reference. (a) dq-axis reference and output current, (b) dq-axis estimated disturbance, and (c) dq-axis reference and output current without a disturbance observer.

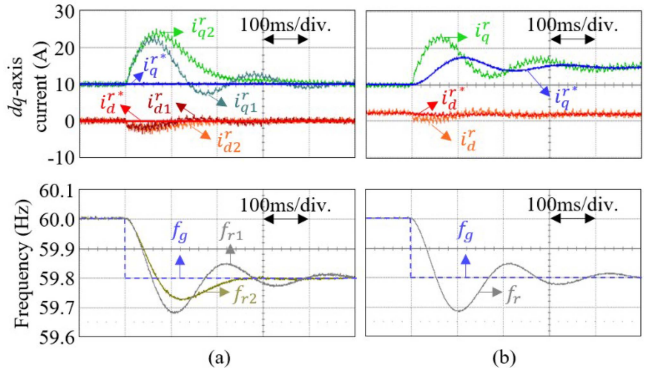

Fig. 10. Responses of CURESYM to a stepped decrease in the grid frequency. (a) Without droop control (1 in subscript: $k_d = 3\ \mathrm{N \cdot m \cdot s/rad}$, 2 in subscript: $k_d = 6\ \mathrm{N \cdot m \cdot s/rad}$) and (b) with droop control ($k_d = 3\ \mathrm{N \cdot m \cdot s/rad}$).

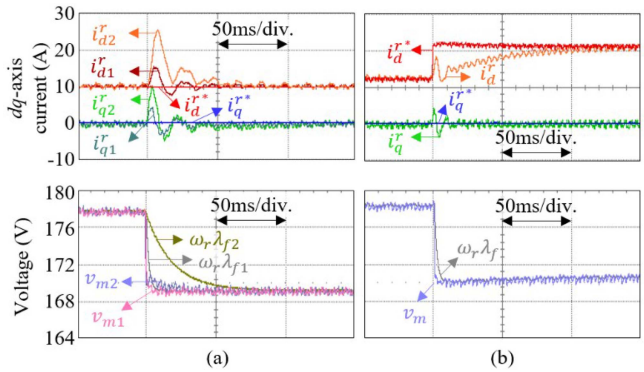

Fig. 11. Responses of CURESYM to a stepped decrease in the grid voltage. (a) Without droop control (1 in subscript: $\omega_{fc} = 2\pi \cdot 100\ \mathrm{rad/s}$, 2 in subscript: $\omega_{fc} = 2\pi \cdot 10\ \mathrm{rad/s}$), (b) with droop control ($\omega_{fc} = 2\pi \cdot 100\ \mathrm{rad/s}$).

estimated by the observer changes, as shown in Fig. 9(b). In addition, when the disturbance observer was deactivated, the current modulating accuracy was degraded, as shown in Fig. 9(c). In the figure, the q-axis current does not have any steady-state error, even without the disturbance observer. This occurs because the swing mechanism of the synchronizer in Fig. 5 adjusts θ_r such that the error between i_q^{r*} and i_q^r is diminished. Consequently, a current regulation error without a disturbance observer is only observed on the d-axis in a steady state.

C. Response to Changes in the Grid Frequency and Voltage

To demonstrate the responses of CURESYM to a change in the grid frequency, the grid frequency is made to drop from 60 Hz to 59.8 Hz by the grid simulator. The d-axis and q-axis current set-points were respectively fixed at zero and 10 A before the frequency drop. Fig. 10(a) shows the responses of CURESYM with two different damping coefficients. Because the droop controller was not applied, i_q^{r*} does not vary according to a frequency change. Although i_q^{r*} is fixed, i_q^r increases at the moment of the frequency drop due to the inertial response emulated by the mechanical part of the synchronizer. The transient response could be adjusted by the damping coefficient k_d. A high k_d mitigates oscillation in the transient response. In a steady state, i_q^r converges back to i_q^{r*}, and the angular frequency of CURESYM f_r is finally synchronized with the grid frequency f_g. In Fig. 10(b), the droop controller was activated, and i_q^{r*} varies depending on the frequency deviation of CURESYM. In a steady state, i_q^r converged to the altered i_q^{r*}.

Fig. 11 shows the responses of CURESYM to the balanced grid voltage sag. The magnitude of the grid voltage was decreased in steps of 0.05 pu. The d-axis and q-axis current set-points were respectively fixed at 10A and zero before the voltage sag. Initially, the droop controller was deactivated in Fig. 11(a). Before the grid voltage increases, the magnitudes of the grid voltage and the SEMF are identical while the output currents are well regulated to the given references. In response to the voltage sag of the grid, the output currents temporarily fluctuate due to the admittance response of (1). However, the currents are quickly settled as $\omega_r\lambda_f$ immediately follows v_m due to the flux controller. The rapid response of the flux controller is helpful in that it strictly regulates the output current. Therefore, CURESYM inherently has tolerance to voltage dips and swells in its current regulation. If droop control is applied, the d-axis current is adjusted further to compensate for the voltage deviation, as shown in Fig. 11(b). Moreover, current reference variations caused by the droop control can easily be limited by the limiters described in Fig. 4, which limit the output current level in a steady state.

In the unbalanced voltage condition, an additional current controller can be combined with CURESYM to mitigate the negative sequence current [27]. In Fig. 12(a), the unbalanced grid voltage was made by adding a negative-sequence voltage ($-0.1\angle 0^\circ$ pu) through the grid simulator. Initially, CURESYM operated without the negative-sequence current

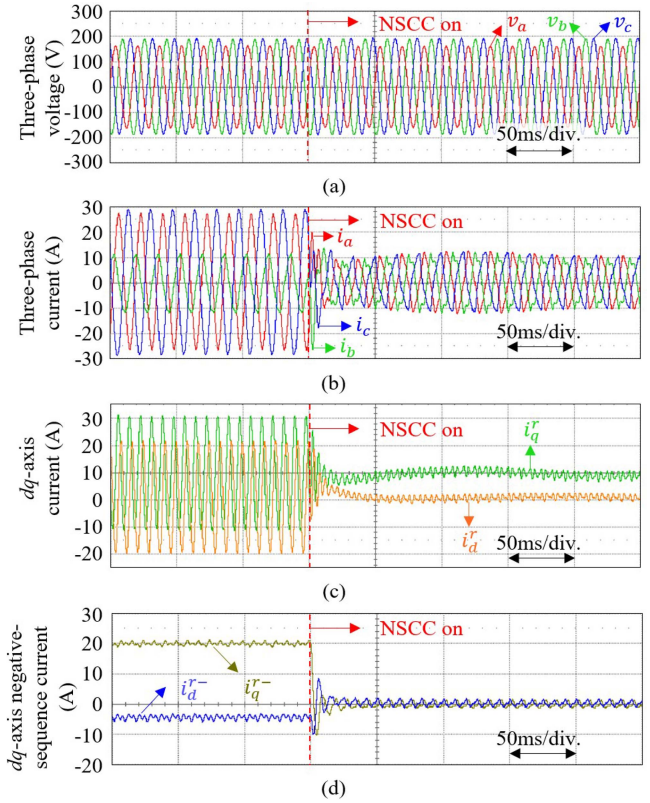

Fig. 12. Experimental result of the unbalanced operation of CURESYM. (a) Three-phase grid voltage, (b) three-phase output current, (c) *dq*-axis output current, (d) *dq*-axis negative-sequence output current.

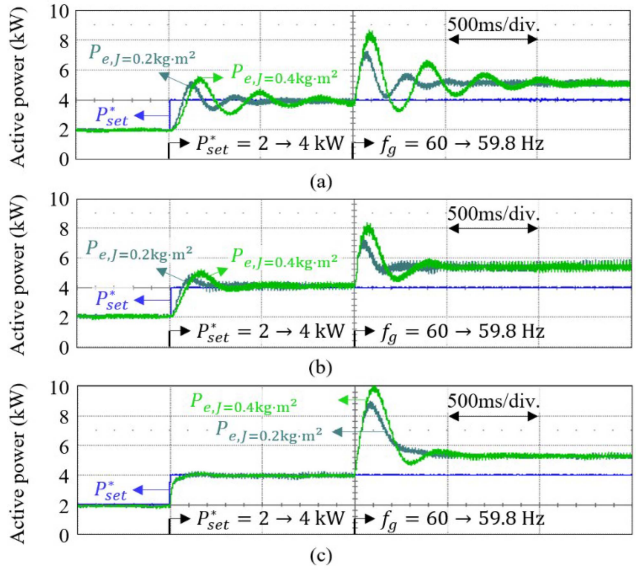

Fig. 13. Comparison of CURESYM's active power response with other VSMs. (a) Synchronverter [13], (b) improved damping method [22], and (c) CURESYM.

controller (NSCC), and the *d*-axis and *q*-axis current set-points were respectively fixed at zero and 10 A. When the NSCC was deactivated, the output three-phase currents were unbalanced as shown in Fig. 12(b) and the second-order harmonics appeared in the *dq*-axis currents as shown in Fig. 12(c). When the NSCC was activated, the *dq*-axis negative-sequence currents i_d^{r-} and i_q^{r-} were rejected as shown in Fig. 12(d). As a result, the second-order harmonics in the *dq*-axis currents and unbalances in the three-phase currents were also effectively removed.

D. Comparisons With Other VSMs

The comparison results with other VSMs in Fig. 13 clearly show how the performance of CURESYM is distinctive. First, a step increase is applied to the active power set-point P_{set}, after which a step decrease in the grid frequency follows sequentially. When using CURESYM, P_{set} determines the *q*-axis current set-point. The droop coefficients used in each topology are identical and are assumed to be fixed for the same steady-state responses. As shown in Fig. 13(a), the responses of the synchronverter [13] under the test scenario had large oscillations. However, adjusting the dynamics was limited, as the damping effect cannot be separately adjusted from the droop coefficient. As shown in Fig. 13(b), an improved damping method [22] could mitigate transient oscillations without affecting the steady-state responses of droop control. However, the transient response to P_{set} was still affected by a change in the inertia coefficient. In Fig. 13(c), it is confirmed that the responses of CURESYM to P_{set} were not affected by either the inertia or the droop coefficients. In this test, τ_{cm} was set to 10 ms as an example, meaning that a very rapid response to P_{set} was also achievable in CURESYM. In addition, the damping coefficient was also designed to have a large value ($k_d = 6\ \mathrm{N\cdot m\cdot s/rad}$). As a result, oscillations due to frequency drops were effectively mitigated without affecting the steady-state responses.

E. Stand-Alone Mode of CURESYM

The proposed method is inherently capable of stand-alone operation without any changes in the control structures. In Fig. 14, after the grid simulator was disconnected by a circuit breaker, CURESYM became the only voltage source in the experimental setup. For this experiment, droop control was activated, and the control parameters in Table II were used as the default condition. Exceptionally, ω_{fc} was set to $2\pi \cdot 10$ rad/s, as an excessive response of the flux controller could lead to voltage instability in the stand-alone mode.

As shown in Fig. 14(a), the grid voltage was robustly maintained by CURESYM in the islanding situation. The output current in the stand-alone mode is determined by the load conditions. Because a resistive load was connected in the experimental setup, the output current of CURESYM mainly exists on the *q*-axis, as shown in Fig. 14(b). In Fig. 14(c) and (d), the frequency and the voltage magnitude in the steady-state were determined by the values of the droop coefficients.

The *d*-axis and *q*-axis current errors between the set-points and the actual outputs determined the voltage deviation and frequency deviation from the nominal values, respectively.

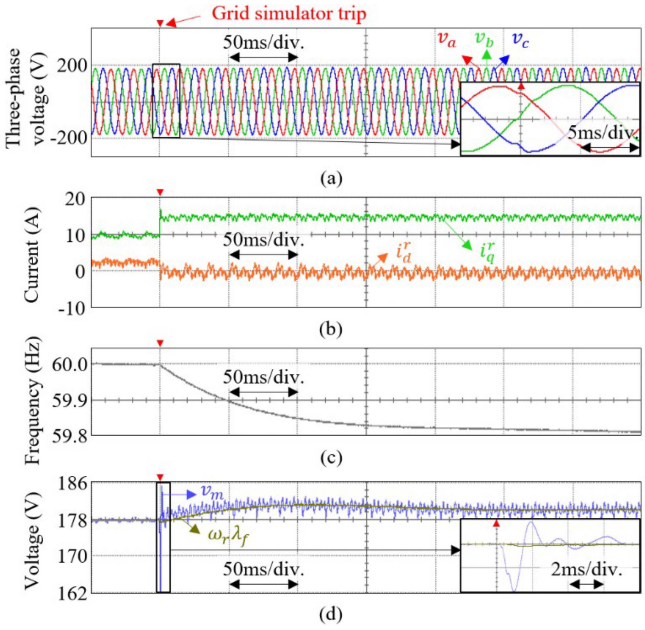

Fig. 14. Responses of CURESYM when transitioning into the stand-alone mode. (a) Three-phase grid voltage, (b) dq-axis output current, (c) angular frequency of CURESYM, and (d) magnitude of the grid voltage and SEMF.

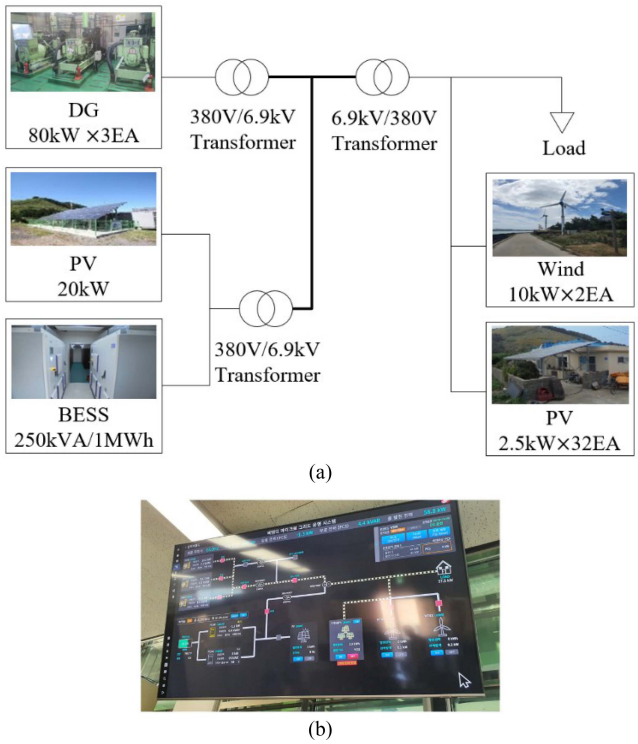

Fig. 15. Biyangdo microgrid. (a) Overall description of the microgrid for the on-site test, and (b) microgrid monitoring panel.

V. On-Site Test Results

A. Test Site

The performance of CURESYM is verified through the on-site test results. The primary objective of CURESYM is to mitigate grid frequency variations by providing inertial responses. However, the laboratory-scale tests mentioned earlier were not enough to assess CURESYM with regard to its primary objective, as the grid simulator operates as an infinite bus, strictly regulating the grid frequency. Therefore, we conducted on-site tests in an actual microgrid to confirm the grid-supporting performance of CURESYM.

The test was conducted on Biyangdo, a small island of Jeju-do in South Korea. The power grid of Biyangdo is an isolated microgrid without interconnections to the main grid of Jeju-do. The Biyangdo grid includes three 80 kW diesel generators (DGs) and RESs consisting of 100 kW photovoltaic (PV) and 20 kW wind generators in total. In addition, a 1 MWh BESS is connected to the grid via a 250 kVA inverter, and CURESYM was implemented in this inverter. An overall description of the Biyangdo grid and photos of the facilities are shown in Fig. 15. The average load during the tests was about 70 kW. When one DG was connected to the grid, the estimated inertia constant [18] and short-circuit ratio (SCR) of the grid were 0.52 s and 6.5, respectively. These values are estimated based on the nominal parameters in Table III, and in particular, the SCR was estimated at the point of common coupling of the BESS-inverter [28]. The waveforms obtained from the on-site tests are captured by a data acquisition system with a sampling period of 200 ms. The parameters for the on-site tests are listed in Table III.

TABLE III
Parameters Used for On-Site Tests

	Parameter	Value
Circuit	Nominal grid frequency	60 Hz
	Nominal grid voltage (L-L)	380 V
	Nominal inverter power: S_n	250 kVA
	L_f	75 μH
	R_f	12 mΩ
Control	J	1.76 kg · m^2
	k_d	17.59 N · m · s/rad
	ω_d	0.5 rad/s
	τ_{cm}	1 s
	ω_{fc}	$2\pi \cdot 10$rad/s
	ω_{eso}	$2\pi \cdot 300$ rad/s
	D_p, D_q	Not applied

B. Test Results

First, the application effect of CURESYM was compared with the conventional constant power control scheme in the GFL mode. The current references in both cases were identically given from the power reference transmitted from the power management system. During the test, a DG and RESs were operated in parallel with the BESS. Figs. 16 and 17 show the waveforms of the grid frequency and the output active power of the inverter, as recorded over one minute in the daytime. The active power reference of the inverter was set to 20 kW. Due to restricted access to accurate measurements and the nominal-value-based references, there could be steady-state errors in general. In the test site, as shown in Fig. 16(a), fluctuations of the grid frequency may be severe due to the low inertia of the diesel generator with

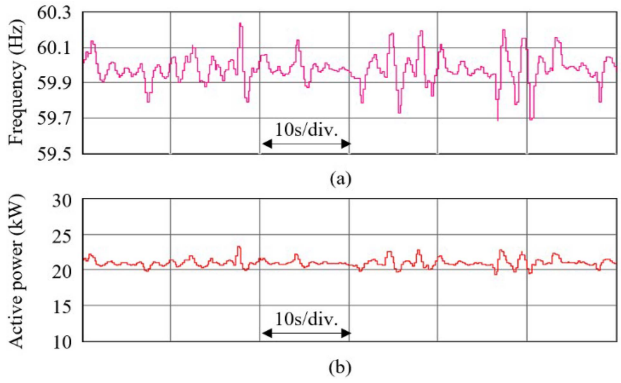

Fig. 16. On-site test results for constant power control with a BESS inverter in a normal situation. (a) Grid frequency, (b) output active power of the BESS inverter.

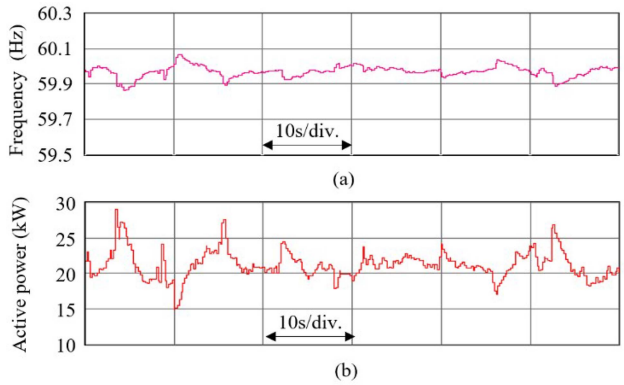

Fig. 17. On-site test result for CURESYM with a BESS inverter in a normal situation. (a) Grid frequency, (b) output active power of the BESS inverter.

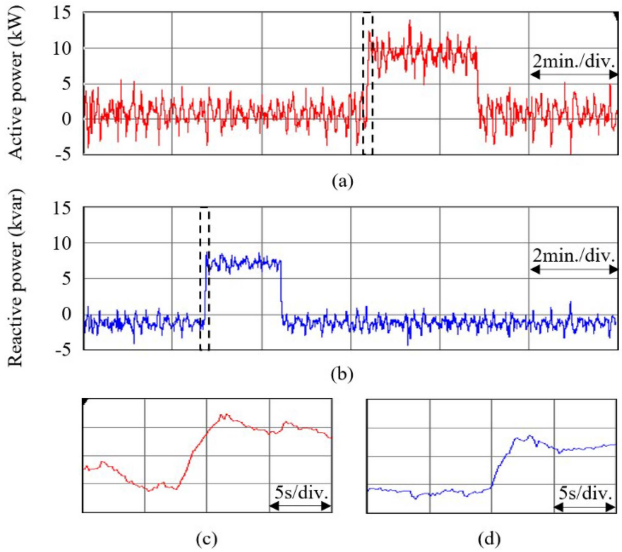

Fig. 18. On-site test result for step responses of the CURESYM to the power reference. (a) Output active power, (b) output reactive power, (c) enlarged view of the step response in active power control, (d) enlarged view of the step response in reactive power control.

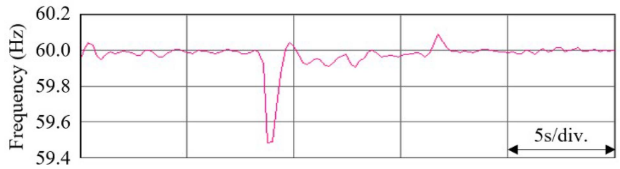

Fig. 19. On-site test result of the grid frequency when a DG is tripped while three DGs operate in parallel and CURESYM is disconnected from the grid.

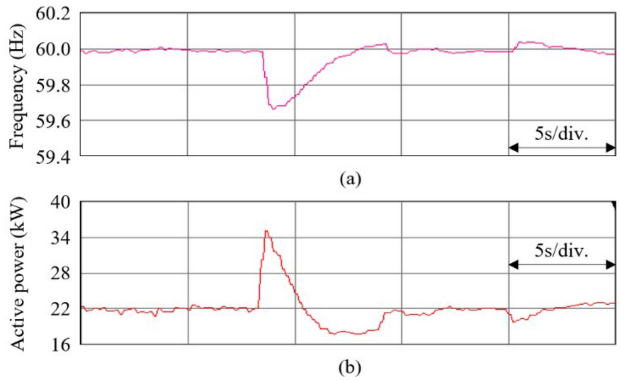

Fig. 20. On-site test result when a DG is tripped while two DGs and CURESYM operate in parallel. (a) Grid frequency, (b) output active power of CURESYM.

abrupt variations of loads and RESs. With constant power control for the inverter, the instantaneous active power remains close to its average, as shown in Fig. 16(b), despite the severe fluctuation of the grid frequency. On the other hand, the degree of variation of the active power in CURESYM is considerable due to the inertial and damping responses, as shown in Fig. 17(b). When comparing Figs. 16(a) and 17(a), it is inferred that CURESYM could effectively stabilize the grid frequency at the expense of fluctuating active power to the grid.

In Fig. 18, the active power reference changes from zero to 8 kW and back to zero. Likewise, the reactive power reference also changes from zero to 8 kvar and back to zero. By virtue of the current modulator, CURESYM can regulate the active power through the q-axis current reference and the reactive power through the d-axis current reference. As shown in Fig. 18, this power modulation scheme through the d-q current is superimposed onto the emulated inertial and damping responses in CURESYM.

Finally, it was considered whether or not CURESYM could partially substitute for synchronous machines. In Fig. 19, one of three active DGs in parallel is intentionally tripped while CURESYM is not connected to the grid. The eliminated DG was delivering 20 kW of active power in constant power mode before the trip event. As shown in Fig. 19, the initial RoCoF and the frequency nadir after the trip were recorded as -1.24 Hz/s and 59.48 Hz, respectively. In Fig. 20, an identical event was repeated while CURESYM was operating with two DGs in parallel. As shown in Fig. 20(b), the active power of CURESYM increases rapidly after the trip event and converges back to the original set-point. In this case, the initial RoCoF and the

frequency nadir are correspondingly −0.99 Hz/s and 59.66 Hz in Fig. 20(a), better than those of the first scenario in terms of frequency stability. That is, CURESYM could help to enhance the frequency stability in this low-inertia grid.

VI. Conclusion

This article proposed a control method denoted as CURESYM for a voltage-source inverter to emulate a synchronous machine with two EMFs and a disturbance observer. CURESYM can separately design dynamic responses to current references regardless of inertia or the damping parameters. Consequently, grid support functions can be offered simultaneously with the intended response to the reference input. Along with the disturbance observer, CURESYM can offer accurate current-regulating performance. The fundamental features of CURESYM were experimentally demonstrated through laboratory-scale experiments. By testing CURESYM in an actual island grid, its grid-supporting performance could be practically assessed. The on-site test results confirm that the proposed method can effectively support weak grids.

References

[1] D. Liu, X. Zhang, and C. K. Tse, "Effects of high level of penetration of renewable energy sources on cascading failure of modern power systems," *IEEE J. Emerg. Sel. Topics Circuits Syst.*, vol. 12, no. 1, pp. 98–106, Mar. 2022.

[2] A. Khan, M. Hosseinzadehtaher, M. B. Shadmand, S. Bayhan, and H. Abu-Rub, "On the stability of the power electronics-dominated grid: A new energy paradigm," *IEEE Ind. Electron. Mag.*, vol. 14, no. 4, pp. 65–78, Dec. 2020.

[3] A. Fernández-Guillamón, E. Gómez-Lázaro, E. Muljadi, and Á. Molina-García, "Power systems with high renewable energy sources: A review of inertia and frequency control strategies over time," *Renewable Sustain. Energy Rev.*, vol. 115, pp. 1–12, Nov. 2019.

[4] L. Badesa, C. Matamala, Y. Zhou, and G. Strbac, "Assigning shadow prices to synthetic inertia and frequency response reserves from renewable energy sources," *IEEE Trans. Sustain. Energy*, vol. 14, no. 1, pp. 12–26, Jan. 2023.

[5] Y. Gui, X. Wang, F. Blaabjerg, and D. Pan, "Control of grid-connected voltage-source converters: The relationship between direct-power control and vector-current control," *IEEE Ind. Electron. Mag.*, vol. 13, no. 2, pp. 31–40, Jun. 2019.

[6] Y. S. Perdana, S. M. Muyeen, A. Al-Durra, H. K. Morales-Paredes, and M. G. Simões, "Direct connection of supercapacitor–battery hybrid storage system to the grid-tied photovoltaic system," *IEEE Trans. Sustain. Energy*, vol. 10, no. 3, pp. 1370–1379, Jul. 2019.

[7] W. Du et al., "Modeling of grid-forming and grid-following inverters for dynamic simulation of large-scale distribution systems," *IEEE Trans. Power Del.*, vol. 36, no. 4, pp. 2035–2045, Aug. 2021.

[8] Z. Miao, A. Domijan, and L. Fan, "Investigation of microgrids with both inverter interfaced and direct AC-connected distributed energy resources," *IEEE Trans. Power Del.*, vol. 26, no. 3, pp. 1634–1642, Jul. 2011.

[9] M. Rasheduzzaman, J. A. Mueller, and J. W. Kimball, "An accurate small-signal model of inverter-dominated islanded microgrids using *dq* reference frame," *IEEE J. Emerg. Sel. Topics Power Electron.*, vol. 2, no. 4, pp. 1070–1080, Dec. 2014.

[10] W. Du et al., "A comparative study of two widely used grid-forming droop controls on microgrid small-signal stability," *IEEE J. Emerg. Sel. Topics Power Electron.*, vol. 8, no. 2, pp. 963–975, Jun. 2020.

[11] H. Nikkhajoei and R. H. Lasseter, "Distributed generation interface to the CERTS microgrid," *IEEE Trans. Power Del.*, vol. 24, no. 3, pp. 1598–1608, Jul. 2009.

[12] Z. Li, C. Zang, P. Zeng, H. Yu, S. Li, and J. Bian, "Control of a grid-forming inverter based on sliding-mode and mixed H_2 /H_∞ control," *IEEE Trans. Ind. Electron.*, vol. 64, no. 5, pp. 3862–3872, May 2017.

[13] Q.-C. Zhong and G. Weiss, "Synchronverters: Inverters that mimic synchronous generators," *IEEE Trans. Ind. Electron.*, vol. 58, no. 4, pp. 1259–1267, Apr. 2011.

[14] K. R. Vasudevan, V. K. Ramachandaramurthy, T. S. Babu, and A. Pouryekta, "Synchronverter: A comprehensive review of modifications, stability assessment, applications and future perspectives," *IEEE Access*, vol. 8, pp. 131565–131589, 2020.

[15] S. Qu and Z. Wang, "Cooperative control strategy of virtual synchronous generator based on optimal damping ratio," *IEEE Access*, vol. 9, pp. 709–719, 2021.

[16] F. Wang, L. Zhang, X. Feng, and H. Guo, "An adaptive control strategy for virtual synchronous generator," *IEEE Trans. Ind. Appl.*, vol. 54, no. 5, pp. 5124–5133, Sep./Oct. 2018.

[17] J. Alipoor, Y. Miura, and T. Ise, "Power system stabilization using virtual synchronous generator with alternating moment of inertia," *IEEE J. Emerg. Sel. Topics Power Electron.*, vol. 3, no. 2, pp. 451–458, Jun. 2015.

[18] W. Du, Q. Fu, and H. F. Wang, "Power system small-signal angular stability affected by virtual synchronous generators," *IEEE Trans. Power Syst.*, vol. 34, no. 4, pp. 3209–3219, Jul. 2019.

[19] X. Xiong, C. Wu, B. Hu, D. Pan, and F. Blaabjerg, "Transient damping method for improving the synchronization stability of virtual synchronous generators," *IEEE Trans. Power Electron.*, vol. 36, no. 7, pp. 7820–7831, Jul. 2021.

[20] J. A. Suul, S. D'Arco, and G. Guidi, "Virtual synchronous machine-based control of a single-phase bi-directional battery charger for providing vehicle-to-grid services," *IEEE Trans. Ind. Appl.*, vol. 52, no. 4, pp. 3234–3244, Jul./Aug. 2016.

[21] S. Dong and Y. C. Chen, "Adjusting synchronverter dynamic response speed via damping correction loop," *IEEE Trans. Energy Convers.*, vol. 32, no. 2, pp. 608–619, Jun. 2017.

[22] M. Ebrahimi, S. A. Khajehoddin, and M. Karimi-Ghartemani, "An improved damping method for virtual synchronous machines," *IEEE Trans. Sustain. Energy*, vol. 10, no. 3, pp. 1491–1500, Jul. 2019.

[23] V. Blasko and V. Kaura, "A new mathematical model and control of a three-phase AC–DC voltage source converter," *IEEE Trans. Power Electron.*, vol. 12, no. 1, pp. 116–123, Jan. 1997.

[24] Y. Park and S.-K. Sul, "A novel method utilizing trapezoidal voltage to compensate for inverter nonlinearity," *IEEE Trans. Power Electron.*, vol. 27, no. 12, pp. 4837–4846, Dec. 2012.

[25] W.-H. Chen, J. Yang, L. Guo, and S. Li, "Disturbance-observer-based control and related methods—An overview," *IEEE Trans. Ind. Electron.*, vol. 63, no. 2, pp. 1083–1095, Feb. 2016.

[26] B. Wang, Y. Xu, Z. Shen, J. Zou, C. Li, and H. Liu, "Current control of grid-connected inverter with LCL filter based on extended-state observer estimations using single sensor and achieving improved robust observation dynamics," *IEEE Trans. Ind. Electron.*, vol. 64, no. 7, pp. 5428–5439, Jul. 2017.

[27] Y. Wang, D. Wang, Z. Huang, and Y. Li, "Hybrid voltage and current control strategy for virtual synchronous generator under unbalanced voltage conditions," *Inst. Eng. Technol. Renewable Power Gener.*, 2022, doi: 10.1049/rpg2.12497.

[28] A. V. Timbus, P. Rodriguez, R. Teodorescu, and M. Ciobotaru, "Line impedance estimation using active and reactive power variations," in *Proc. IEEE Power Electron. Specialists Conf.*, 2007, pp. 1273–1279.

Geon Heo (Graduate Student Member, IEEE) was born in Busan, South Korea. He received the B.S. degree in mechanical and control engineering from Handong Global University, Pohang, South Korea, in 2018. He is currently working toward the Ph.D. degree in integrated energy technology with the Graduate School of Energy Convergence, Gwangju Institute of Science and Technology, Gwangju, South Korea. His current research interests include modeling and control of power conversion systems.

Yongsoon Park (Member, IEEE) received the B.S., M.S., and Ph.D. degrees in electrical engineering from Seoul National University, Seoul, South Korea, in 2008, 2010, and 2015, respectively. From 2015 to 2016, he was a Senior Engineer with Samsung Electronics Company, Ltd., South Korea. Since 2016, he has been with the Gwangju Institute of Science and Technology, Gwangju, South Korea, where he is currently an Associate Professor. His current research interests include design and control of power conversion circuits for grid connection and motor drives.

Kyungkyu Lee was born in Seongnam, South Korea. He received the B.S. and M.S. degrees in electrical engineering from Chungbuk National University, Cheongju, South Korea, in 2014 and 2016, respectively. He is currently a Researcher with Korea Electric Power Research Institute, Daejeon, South Korea. His current research interests include power electronics, power quality problems and solutions, energy storage system, renewable energy and microgrid systems.

Hoseon Ryu was born in Daejeon, South Korea. He received the B.S., M.S., and Ph.D. degrees in electrical engineering from Chungnam National University, Daejeon, South Korea, in 1993, 1995, and 2015, respectively. Since 1995, he has been with the Korea Electric Power Research Institute as a Chief Researcher. He was also a Visiting Scholar with Virginia Tech, Blacksburg, VA, USA, and Florida State University, Tallahassee, FL, USA, in 2003 and 2008, respectively. His research interests include power electronics and its application like distributed generation system, micro grid, grid stability and control of large power converter.